Research Article Vol. 4, No. 2 / 15 February 2021 / OSA Continuum 650

Second derivative diffuse reflectance spectroscopy for estimating tissue hypoxia

WESAM BACHIR[1,2,*] AND OMAR HAMADAH[3,4]

[1] Biomedical Photonics Laboratory, Higher Institute for Laser Research and Applications, Damascus University, Damascus, Syrian Arab Republic
[2] Faculty of Informatics Engineering, Al-Sham Private University, Damascus, Syrian Arab Republic
[3] Department of Oral Medicine, Faculty of Dental Medicine, Damascus University, Damascus, Syrian Arab Republic
[4] Higher Institute for Laser Research and Applications, Damascus University, Damascus, Syrian Arab Republic
[*] w.b.foit@aspu.edu.sy

Abstract: Estimating tissue hypoxia using diffuse reflectance spectroscopy has been a tough challenge. In this work, a novel approach for extracting tissue oxygen saturation (StO_2) from diffuse reflectance spectra is presented. The devised method is based on the second derivative of visible light diffuse reflectance of tissue over 100 nm ranged from 500 nm to 600 nm. The theoretical predictions of the method were confirmed by estimating StO_2 from simulated diffuse reflectance generated by Monte Carlo based look-up tables. Effect of scattering and blood volume fraction on the StO_2 estimation are quantified. Validation was also tested on clinical measurements from oral mucosal tissue. The devised second derivative Diffuse reflectance spectroscopy (SD-DRS) shows a potential application for detecting tumor hypoxia, in particular, the differentiation between healthy and cancerous tissue.

1. Introduction

Tissue oxygen saturation (StO_2) is a key physiological parameter and a reliable marker of disease activity by which oxygen delivery and uptake in biological tissue can be assessed. Thus, tissue oxygenation is an indicator of tissue viability and functionality [1]. Abnormality in tissue oxygenation can vary due to different pathologies and disorders such as diabetes, cardiovascular diseases and cancer. Lately, local measurement of tissue oxygen saturation StO_2 has been of paramount importance particularly, for early detection of malignant tumors that has proven to substantially reduce the mortality rate from cancer worldwide [2].

There exists a number of different modalities for measuring tissue oxygen saturation [3]. However, optical techniques have attracted a growing interest as a noninvasive technology. A commonly used optical method for quantifying StO_2 is Near infrared spectroscopy (NIRS). Although, it has been extensively used due to its high penetration depth in tissue as well as robustness and ease of use, NIRS requires large source-detector separation making it unsuitable for local tissue oximetry. Additionally, the in vivo precision of NIRS-based oximetry has repeatedly been reported to be insufficient for clinical practice [4] despite recent advancement to improve its clinical outcomes [5].

Alternatively, diffuse reflectance spectroscopy (DRS) has been a promising modality that provides valuable information about the optical properties of biological tissue of interest. Recently, physiological parameters particularly oxygen saturation and blood volume fraction in tissue have been reliably used for detecting tissue hypoxia that is associated with malignancy and cancer in many organs of human body [6]. However, research on estimating tissue hypoxia has been mostly restricted to limited number of analytical or empirical models [7]. For example, a quadratic polynomial fit algorithm for estimating StO_2 in human white brain matter from diffuse reflectance

#410807 https://doi.org/10.1364/OSAC.410807
Journal © 2021 Received 23 Sep 2020; revised 26 Dec 2020; accepted 28 Jan 2021; published 2 Feb 2021

OSA CONTINUUM

spectra was developed by Rejmstad et al. [8]. The second spectral derivative approach in near infrared diffuse spectroscopy was first introduced by Cooper et al. [9] as a noninvasive modality for measurement of absolute cerebral deoxyhemoglobin concentration and mean optical path length in the neonatal brain. More recently, Yeganeh et al. [10] used first and second derivatives in near infrared region for measuring baseline values and changes in the tissue chromophore concentrations.

Previously, research has focused on utilizing near infrared spectroscopy for estimating total hemoglobin and oxygen saturation or a combination of visible and near infrared spectroscopy. Brouwer de Koning et al. [11] investigated diffuse reflectance spectroscopy over broad wavelength range from 400 to 1600 nm for discriminating oral cavity tumor from healthy oral mucosal tissue as a guiding tool for oral cancer excision.

This focus has been shifted lately to the use of visible spectroscopy for tissue diagnosis. Chen et al. [12] presented a method for estimating oxygen saturation from diffuse reflectance spectra using differential wavelet transformation. Also, Hu et al. [13] provided a rapid ratiometric analysis for estimating tissue hemoglobin concentration and oxygen saturation from measured tissue diffuse reflectance spectra at specific wavelengths in the visible range of spectrum. In addition, Nasseri et al. [14] developed OxyVLS oximeter based on visible light for measuring tissue oxygen saturation StO_2 locally and independent of scattering. However, it has not been proven clinically.

In this paper, we present a simple yet effective method to extract tissue oxygen saturation in the visible wavelength range from 500 to 600 nm based on characteristics of second derivative peaks of diffuse reflectance spectra. Tissue blood volume fraction and scattering effects on StO_2 are analyzed and discussed.

2. Materials and Methods

2.1. Theory

It is well known that hemoglobin can be considered a primary absorber for skin and epithelial tissue where tumors develop most. Diffuse reflectance spectra from hemoglobin are characterized by two dips and two humps related to oxygenated hemoglobin and deoxygenated hemoglobin as shown in Fig. 1(a) in which spectra were plotted using data taken from [15]. Also, the area of these humps and dips can be varied with different concentration of oxygenated and deoxygenated hemoglobin and thus reflect the variation in tissue oxygen saturation. The dips are featured by two specific wavelengths 543 and 577 nm as presented in Fig. 1(b).

Mathematically, either dip characterizing the diffuse reflectance spectrum, in the 500 to 600 nm range, can be modeled as a reversed gaussian function expressed as

$$DRS(\lambda) = -Ae^{-\frac{(\lambda-\lambda_0)^2}{2\Delta\lambda^2}} \tag{1}$$

where, A represents the amplitude of the dip, λ_0 is the wavelength corresponding to the location of the peak center, and $\Delta\lambda$ is a parameter for controlling the width of the dip as shown in Fig. 1(c) in the upper graph. The first derivative (FD) of the diffuse reflectance spectra in the above mentioned wavelength range can be described by its rate of change or reflectance with respect to wavelength.

Therefore, the second derivative (SD) is by definition the rate of change of the slope, thus, representing the curvature of the spectrum. Consequently, the first and second derivatives can provide information on morphological variations in diffuse reflectance over this range and hence indirect evaluation of tissue oxygen saturation.

As for diffuse reflectance, the FD is the rate of change of reflectance with respect to wavelength. It starts and finishes at zero. It also passes through zero at a wavelength that corresponds to the maximum of the reflectance as can be seen in Fig. 1(c) in the middle graph.

OSA CONTINUUM

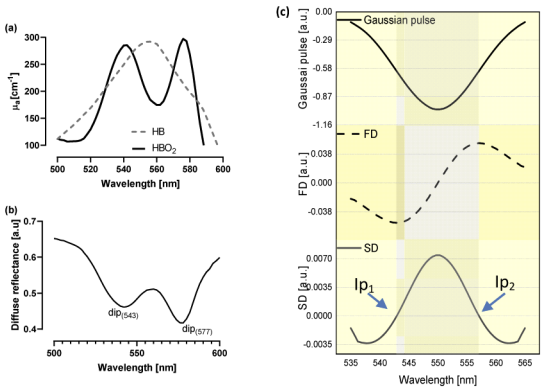

Fig. 1. (a) Deoxygenated and oxygenated hemoglobin absorption spectra in the wavelength range 500–600 nm. (b) Diffuse reflectance spectrum of hemoglobin marked by varying areas of the oxygenated hemoglobin dips, $dip_{(543)}$ and $dip_{(577)}$. (c) Upper: reversed gaussian pulse. Middle: first derivative of the pulse. Lower: second derivative of the pulse characterized by inflection points Ip_1 and Ip_2.

Either side of this point are positive and negative bands with maximum and minimum at the same wavelengths as the inflection points Ip_1 and Ip_2 in the reflectance as shown in Fig. 1(c) in the lower graph.

For second order derivative, the most characteristic feature is a positive band with maximum at the same wavelength as the minimum on the zero-order DRS. It can also be noted that the peak area in the SD of reflectance that is bounded by the inflection points is directly proportional to the size of the area of the gaussian pulse. The following Eqs. (2) and (3) can be used to compute the first and second derivatives ($DRS'(\lambda)$ and $DRS''(\lambda)$ respectively). They are based on the central difference approximation to the FD and SD of diffuse reflectance spectrum, given by

$$DRS'(\lambda) = dDRS/d\lambda \simeq (DRS(\lambda + h) - DRS(\lambda - h))/2h \tag{2}$$

$$DRS''(\lambda) = d^2DRS/d\lambda^2 \simeq (DRS(\lambda + h) - 2DRS(\lambda) + DRS(\lambda - h))/h^2 \tag{3}$$

where h is the step length. The resulting peak area can also be calculated by integrating the second derivative over an interval defined by the inflection points Ip_1 and Ip_2 given by the following formula

$$Area = \int_{Ip_1}^{Ip_2} DRS''(\lambda)d(\lambda) \tag{4}$$

In this work FD, SD, and the area were calculated numerically using MATLAB 2016 (Mathworks Inc.).

To simulate diffuse reflectance in a semi-infinite single layer tissue model, a look-up table based on Monte Carlo simulation MC-LUT [16] was created for the forward model. Although, a number of different methods exist for generating diffuse reflectance spectra, in this study MC-LUT method was preferred over others as it is more accurate than experimental LUT and diffusion approximation-based methods. Also, with advanced computational capabilities, it has become easier to implement and more importantly can be adapted to more complex probe and tissue geometries [16]. In the MC-LUT used in this work, the absorption coefficient spanned from 0.1 to 35 cm^{-1} with 10 increments (0.1,0.5,1,5,10,15,20,25,30,35). Likewise, the reduced scattering coefficient spanned from 0.1 to 35 cm^{-1} with 10 increments (0.1,0.5,1,5,10,15,20,25,30,35). Interpolation between values in the LUT, with 50 points across absorption and scattering ranges selected, was implemented by cubic splines. 10^6 photons were used for all simulations using MC-LUT.

OSA CONTINUUM

The reduced scattering coefficient used in the forward model [17] was expressed by

$$\mu_s^{/}(\lambda) = \mu_s^{/}(\lambda_0).(\frac{\lambda}{\lambda_0})^{-B} \tag{5}$$

where λ_0 is 600 nm and B is the scattering power. The absorption coefficient was calculated by the following expression [18]

$$\mu_a(\lambda) = \sum_{i=1}^{N} ln(10)\varepsilon_i(\lambda)C_i \tag{6}$$

where $\varepsilon_i(\lambda)$ is the extinction coefficient of a given chromophore, C_i is the concentration of that chromophore, and N is the number of chromophores. The chromophores assumed in tissue in this work were oxygenated hemoglobin and deoxygenated hemoglobin. Then, MC-LUT was used to generate a modeled reflectance spectrum followed by interpolation using cubic splines. The anisotropy coefficient (g-factor) value for tissue was set at 0.9 for all simulations. Although optical properties together with physiological parameters such as blood volume fraction and StO_2 are all affected by anisotropy factor [19], the choice of this value was based on the finding of previous work of Graaff et al. [20]. They found that all values of g factor larger than 0.8 will be the same for any values of scattering coefficient and g factor that generate the same reduced scattering coefficient. Therefore, the assumptions regarding anisotropy in this study are reasonable and justified as also reported by Hennessy et al. [16].

For the simulation study, it was assumed that the refractive index of the tissue matched that of the fiber and was set to 1.4. This assumption was based on the fact that the fiber core material is silica fixed in epoxy (for all illumination and collection fibers simulated) with a refractive index of 1.4 and the refractive index of tissue is nearly 1.37. The reflectivity of the stainless-steel housing tube of the fiber probe was not considered in the simulation study. In fact, our specific probe geometry used in the experimental measurements was taken into account in the simulation where the following probe parameters were considered: number of fibers (one for illumination and six for collection), diameter of all illumination and collection fibers is the same that is, 200 µm, the distance from the center of the illumination fiber to the center of the collection fiber was set to 250 µm. Numerical aperture for all fibers was set to 0.22.

2.2. Experimental setup

In order to evaluate the performance of the proposed approach in clinical settings, Diffuse reflectance spectra of oral mucosal tissue were acquired for which clinical measurements were taken from different locations of the suspicious site inside the oral cavity. All clinical investigations conducted in this work were approved by the ethical committee at Damascus university and in accordance with Helsinki guidelines. Informed consent was also obtained from all subjects prior to DRS measurements. Diffuse reflectance spectra were collected using a compact and portable spectrometer (USB4000 FL, Ocean Optics Inc., Dunedin, FL, USA). For Illumination of the examined tissue, a broadband light source from 400 to 2000nm (HL-2000-FHSA-HP, Ocean Optics Inc., Dunedin, FL, USA) was used.

A bifurcated bundle probe (six fibers for collection around one central fiber for illumination) was used to deliver the light to tissue and collect the diffuse reflected light from within the tissue back to the spectrometer as illustrated in Fig. 2(a). The fibers were made from silica and housed in stainless steel tube. The fiber diameter of the illuminating fiber was 200 µm, six collection fibers with diameter of 200 µm each, and a collection-illumination separation (from center to center) was 250 µm. Diffuse reflectance measurements were calibrated before each session using a reflectance standard (WS-1, Ocean Optics Inc., Dunedin, FL, USA).

The spectrometer was connected to a laptop for controlling the spectroscopic system via Spectrasuit software (Ocean Optics Inc., Dunedin, FL, USA) and then the collected spectra were

OSA CONTINUUM

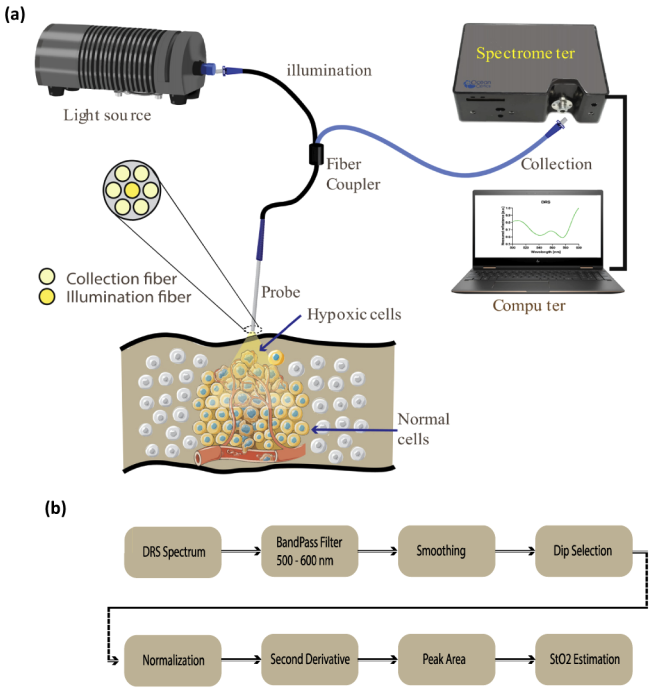

Fig. 2. (a) Schematic view of the optical setup for second derivative diffuse reflectance Spectroscopy (SD-DRS). (b) Workflow of the second derivative spectroscopy analysis of DRS spectra for StO_2 evaluation.

further processed and analyzed offline using MATLAB. Immediately after performing the optical measurements, a mucosal biopsy from the measurement site was taken for histopathological evaluation by a single pathologist blinded to the optical measurement.

Figure 2(b) shows the workflow of StO_2 estimation. The measured reflectance spectra were preprocessed using a Savitzky-Golay filter to smooth the spectrum. SG filter window length and polynomial order used in this study were 7 and 2 respectively. This was followed by spectral normalization by dividing the spectrum by its maximum value over the wavelength range of interest from 500 to 600 nm. Then, FD and SD were calculated numerically using MATLAB and based on Eqs. (2) and (3). Further peak analysis including area calculation was accomplished using Eq. (4) and hence, the StO_2 can be estimated in relation to the area of $dip_{(543)}$ and $dip_{(577)}$.

3. Results

The efficiency of the proposed method to extract StO_2 was evaluated in simulated DRS spectra where level of oxygen saturation ranged from 10–100%. Figure 3 shows an example of the generated forward model of diffuse reflectance.

Optical properties used in this simulation study are as follows: total hemoglobin expressed as blood volume fraction (BVF): 2%, the scattering power B was set at 1.2, and $\mu_s'(\lambda_0)$ was given a value of 17 cm^{-1}. Also, BVF (2%) was selected as it represents the blood volume fraction in skin and epithelial tissue for normal tissue.

Reduced scattering coefficient (17 cm^{-1}) was also selected as an average value that represents different types of biological tissue. Both selected values fall within ranges of these parameters found in the literature for experimental measurements. These values were taken from the literature and considered normal values for healthy tissue [17].

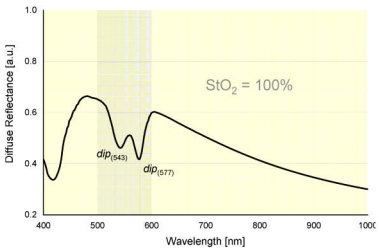

Fig. 3. Simulated diffuse reflectance spectrum for 100% oxygen saturation.

After running the simulation, a set of diffuse reflectance spectra for each oxygenation level from 10% to 100% were generated. Equations (5) and (6) were used in the simulation process to generate the diffuse reflectance DRS spectra for different levels of StO_2. Afterwards, the first and second derivatives of the DRS spectra were determined in MATLAB and the area under the curve corresponding to $dip_{(543)}$ and $dip_{(577)}$ was calculated by numerical integration in MATLAB. For numerical integration, the wavelength interval for each area is defined by the width of the area that is determined using the first derivative as mentioned earlier. The number of integration points is the number of wavelengths occupied by the width of the peak (i.e., wavelength resolution on the x-axis which was 1 nm in this study).

Figures 4(a) and 4(b) show computed area of the second derivative spectrum as a function of the tissue oxygen saturation StO_2 for both $dip_{(543)}$ and $dip_{(577)}$. Where area 1 is the area of the second derivative peak corresponding to $dip_{(543)}$ and its width is defined by the inflection points that are determined by the first derivative. Likewise, area 2 is the area of the second derivative peak corresponding to $dip_{(577)}$ and its width is defined by the inflection points that are determined by the first derivative.

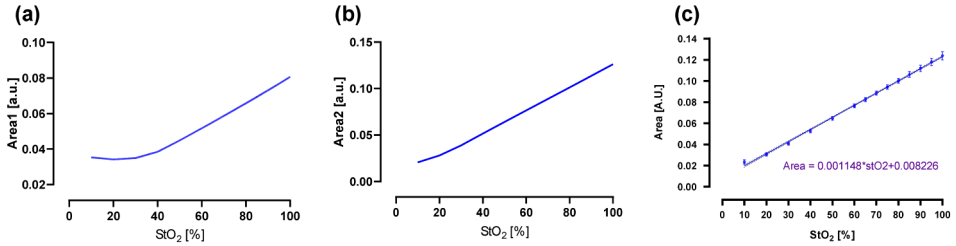

Fig. 4. (a) Calculated area1 as a function of StO_2. (b) Calculated area 2 as a function of StO_2. (c) Calculated area corresponding to $dip_{(577)}$ as a function of the tissue oxygen saturation StO_2 with varying levels of reduced scattering coefficient.

It can be observed that oxygen saturation is directly proportional to both areas of second derivative of oxygenated hemoglobin dips. However, one can notice that the first area values of the second derivative cannot be clearly differentiated for low levels of oxygen saturation ($StO_2 < 30\%$). Since $dip_{(577)}$ is narrower and of higher amplitude compared to $dip_{(543)}$ as shown previously in Fig. 1(a), the focus on this study will be on $dip_{(577)}$ of diffuse reflectance spectrum.

3.1. *Effect of scattering*

To investigate the effect of scattering on the evaluation of tissue saturation, the analysis workflow shown in Fig. 2(b) was implemented for different values of reduced scattering coefficient (at 600 nm) that cover the measured values for healthy and diseased biological tissue i.e. in the range of 5- 40 cm^{-1}. This range was selected based on literature data regarding scattering coefficients

OSA CONTINUUM

for different biological tissue collected by Jacques, S. [17]. The selected range represents most of scattering coefficients of different biological tissue. Consequently, the computed area of the second derivative of $dip_{(577)}$ as a function of the oxygen saturation is demonstrated in Fig. 4(c). A simple linear regression model was fitted to the data to investigate the relationship between StO_2 level and the area of the second derivative peak corresponding to $dip_{(577)}$.

Figure 4(c) confirms a very strong positive linear relationship between the two and a simple linear regression showed a significant relationship between StO_2 and area of the peak corresponding to $dip_{(577)}$ ($p < 0.001$). The linear fitting model is given by the following formula

$$Area = 0.001148 * StO_2 + 0.008226 \tag{7}$$

This model can be used to estimate the level of oxygen saturation after computing the area of the second derivative peak corresponding to $dip_{(577)}$. Figure 5 shows three oxygen saturation levels 10%, 50%, and 100% estimated using Eq. (7) for three simulated diffuse reflectance spectra.

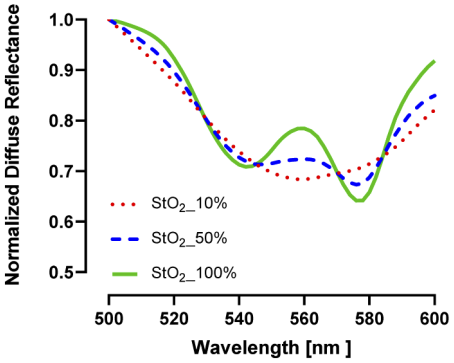

Fig. 5. Simulated diffuse reflectance spectra in the wavelength from 500 to 600 nm for different levels of StO_2 while the BVF was set at 2%.

3.2. *Effect of blood volume fraction*

In order to quantify the effect of the blood volume on the presented method, a similar analysis workflow was repeated and tissue saturation was estimated using second derivative for different blood volume fraction levels ranged from 0.1% to 7% as this range represents BVF values in different pathological conditions. Zhong et al. [21] showed that the blood volume in skin of different types is around 1.5%. Also, the selected range represents different pathophysiological conditions such as cancer especially epithelial tissue where tumors develop mostly as reported by Amelink et al. [22]. They found that for normal oral tissue, the average BVF value was 3.6 and 4.1% for tumors on average.

Figure 6 shows a sample of simulated diffuse reflectance spectra in the visible window i.e. from 500 to 600 nm for different levels of BVF and different levels of StO_2.

It can be noticed that diffuse reflectance spectra are dependent on BVF as well as StO_2 levels. As a result, the effect of BVF has to be considered for reliable evaluation of StO_2. To that end, the reflectance value at $dip_{(577)}$ can be used as a spectral feature for quantification of BVF in tissue. This value is related to BVF for a given oxygen saturation level. Also, this value, representing the variation in intensity of normalized reflectance, is directly proportional to StO_2 for a given level of BVF as visualized in Fig. 6.

Once the BVF level is determined, the StO_2 based on second derivative of $dip_{(577)}$ can be estimated. To compare the performance of the proposed method, the analysis workflow mentioned above was applied to estimate StO_2 at different levels of BVF (1,3,5, and 7%).

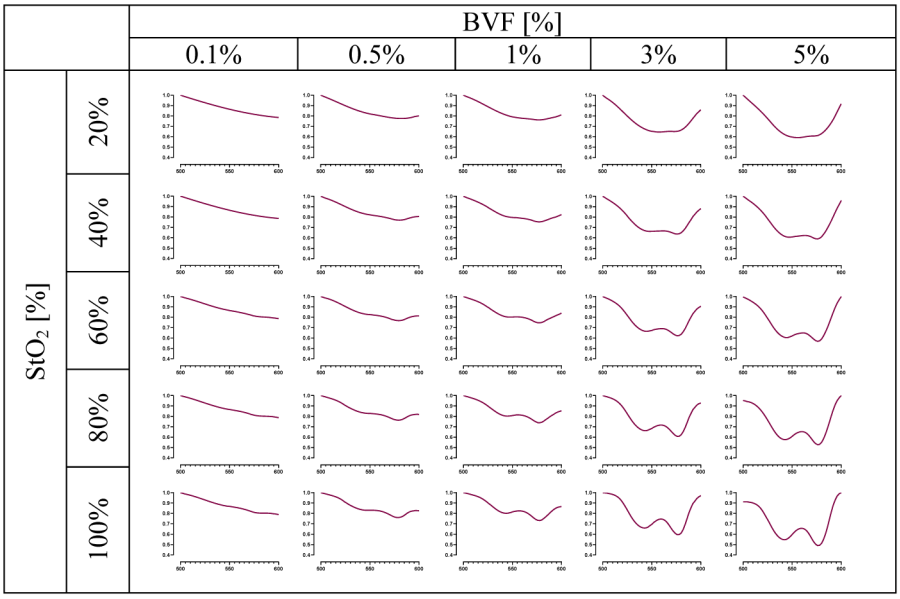

Fig. 6. Simulated diffuse reflectance spectra in the subrange from 500 to 600 nm for different BVF levels and for different StO_2 levels. Vertical axis denotes the normalized reflectance in all graphs.

Diffuse reflectance spectra in the wavelength range of interest with increasing levels of BVF are displayed in Fig. 7(a) for different levels of StO_2. Likewise, Fig. 7(b) shows a linear relationship between computed area and StO_2 for different levels of blood volume. It is evident from Fig. 7(a) that change in reflectance is remarkably larger with increased levels in blood volume fraction as expected. On the other hand, Fig. 7(b) illustrates the trend of calculated area as a function of StO_2 over the range of blood volume fraction levels examined. It is clearly evident from Fig. 7(b) that smaller area of SD-DRS that corresponds to low level of StO_2 is relatively independent on BVF. This is particularly important for tissue hypoxia in tumors. As tissue oxygenation levels increase in tissue, this dependency becomes remarkably higher.

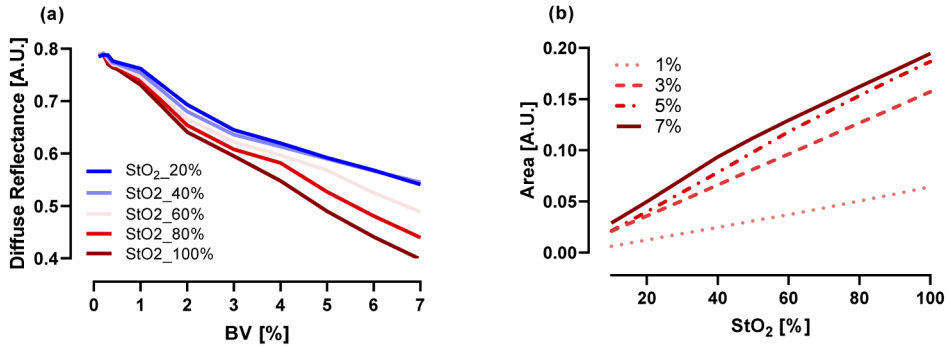

Fig. 7. (a) Diffuse reflectance at $dip_{(577)}$ as a function of BVF for different StO_2 levels. (b) Calculated Area of second derivative of $dip_{(577)}$ as a function of StO_2 for different levels of BVF.

Another effective way to quantify the variation of intensity of diffuse reflectance (for both normalized and non-normalized reflectance) over the whole range from 500 to 600 nm is by

OSA CONTINUUM

calculating the area in which the variation in reflectance intensity occurs. For DR spectra measurements in this work, BVF was estimated by calculating the area of trapezium defined by the diffuse reflectance spectra. The left and right sides (vertical) of the trapezium are parallel and located at the 500 nm and 600 nm on the wavelength axis. The lower side of the trapezium is horizontal and located at the minimum value of DRS intensity on the reflectance axis. Finally, the upper side of the trapezium is defined by the line that connects the reflectance at 500 nm and the reflectance at 600 nm as depicted in Fig. 8.

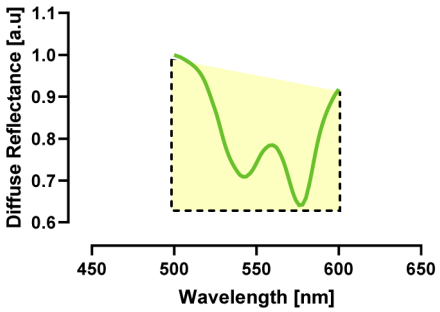

Fig. 8. BVF evaluation by calculating the area of the trapezium covering the diffuse reflectance variation in the wavelength range from 500 to 600 nm.

Consequently, area of SD-DRS at $dip_{(577)}$ can be evaluated as a sparse matrix mapped to BVF and StO_2 space. This matrix can be used to estimate StO_2 for a given value of BVF and computed area of SD-DRS at $dip_{(577)}$. In other words, the area of SD-DRS of $dip_{(577)}$ is a function of BVF and StO_2.

Once the BVF is determined (by calculating the area of trapezium as described above) and the area of SD-DRS at $dip_{(577)}$ is calculated, the corresponding StO_2 can be interpolated from the 2D matrix with varying levels of BVF horizontally and varying levels of StO_2 vertically together with area of SD-DRS at $dip_{(577)}$ values assigned to each element of the matrix.

3.3. Application to clinical diffuse reflectance spectra

The SD-DRS presented in this work was validated on experimental data collected from realistic clinical measurements taken from oral mucosal tissue for both healthy oral tissue as well as benign and malignant oral lesions.

Figure 9(a) displays the estimated StO_2 level in three measured diffuse reflectance spectra from mucosal tissue. One can notice the remarkable association between StO_2 and the shape of spectrum, in particular the flattened oxygenated hemoglobin dips i.e., $dip_{(543)}$ and $dip_{(577)}$ as the StO_2 decreases.

Some recruited patients had multiple lesions in the oral cavity but only measured spectra from lesions that were histopathologically proven were included in the analysis. The sample was divided into three groups. These are: normal (n=117), benign (n=47), and dysplasia/cancer (n=21). The results presented in Fig. 9(b) indicate that good discrimination between all groups is possible with the SD-DRS. A Kruskal-Wallis test provided very strong evidence of a difference ($p < 0.0001$) between the mean ranks of the three tissue groups. A multiple comparison test (two-stage linear step-up procedure of Benjamini, Krieger and Yekutieli) showed significant difference between groups.

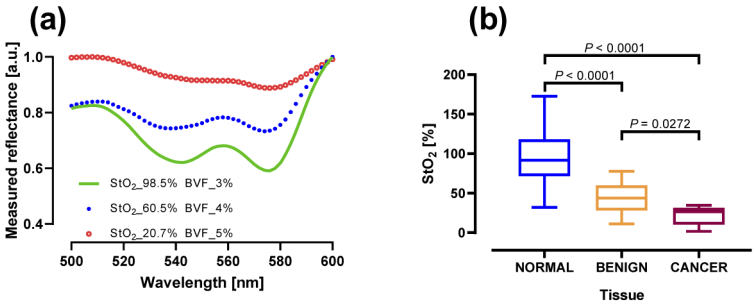

Fig. 9. (a) Estimated StO_2 for different measured diffuse reflectance spectra. (b) Estimated StO_2 using SD-DRS for healthy, benign, and cancerous tissues.

4. Discussion

In this work, a straightforward spectroscopic method for quantitative evaluation of tissue oxygen saturation StO_2 is presented. The method based on second derivative spectroscopy was used to convert the resulting spectral feature into StO_2 values. To the best of our knowledge this is the first study that demonstrates the capability of SD-DRS to estimate tissue oxygen saturation using a simple measuring method.

By observing the shape of diffuse reflectance spectrum in the wavelength range from 500 to 600 nm, one can see that 100% of StO_2 is corresponding to "w" shape of the spectrum [23] and 0% of StO_2 is corresponding to "U" shape of the spectrum as a result of disappearance of $dip_{(543)}$ and $dip_{(577)}$. This was demonstrated with our findings as displayed in Figs. 5 and 9(a) for both simulated and measured DRS. However, for spectra corresponding to StO_2 levels lower than 10%, one can still see a little difference in shape between these spectra resulting in slight difference in the calculated area 2. In fact, the "U" shape for StO_2 levels that are lower than 10% change towards a "V" shape instead of "U" shape as shown in Fig. 10(a). This can be explained by the fact that, for very low levels of StO_2 (from 0 to 10%), deoxygenated hemoglobin becomes the dominant chromophore for which the diffuse reflectance minimum can be seen at 560 nm featuring the absorption peak of deoxygenated hemoglobin. As a result, it can be said that the SD-DRS method exhibits lower differentiation capability for StO_2 level below 10% in comparison to higher levels.

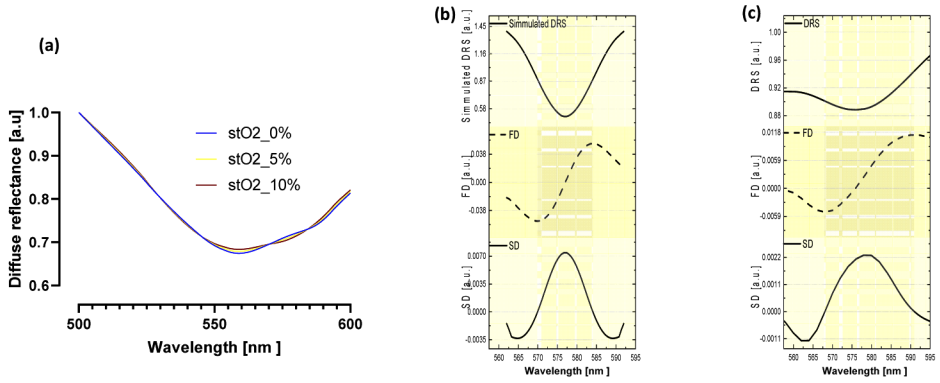

Fig. 10. (a) Simulated diffuse reflectance spectra for low levels of StO_2. (b) $dip_{(577)}$ of Simulated DRS and its first and second derivatives, FD and SD repectively. (c) $dip_{(577)}$ of measured data from oral tissue and its first and second derivatives.

OSA CONTINUUM

Although, spectral analysis applied to the first dip should theoretically give similar results to the second dip, values of StO_2 can be estimated robustly over wider range of tissue oxygenation using $dip_{(577)}$. This may be attributed to the narrower FWHM and higher amplitude of the $dip_{(577)}$ compared to $dip_{(543)}$. Another reason for opting for the second dip is that it can be distinctly identified in clinically measured diffuse reflectance spectra as was observed in the measured spectra.

As mentioned earlier, the developed SD-DRS assumed that hemoglobin is the dominant absorber in simulated reflectance however, in vivo measurements on oral tissue and on other types of tissue in general, different physiological absorbing structures may affect the shape of the reflectance, that is, the characteristics of the gaussian peaks that mimic the dips of the oxygenated hemoglobin can be altered in shape. Figures 10(b) and 10(c) depict the difference between first and second derivative of $dip_{(577)}$ in simulated DRS and first and second derivatives of $dip_{(577)}$ in measured DRS from oral mucosal tissue. Clearly, the dip in measured DRS becomes more flattened, with larger FWHM, and asymmetric in relation to 577 nm wavelength. This demonstrates the contribution of other absorption and scattering effects to the measured DRS. This in turn, may lead to wider range of StO_2 and possibly unexpected results relating to the extreme unphysiological values of StO_2. However, one possible way to rectify this could be by introducing a correction factor based on experimental measurements using optical phantoms with pre-set values of StO_2 and BVF. Furthermore, the estimation procedure worked well for the simulated reflectance in this study but for some real DRS measurements this has not been the case. This can be explained primarily by the difference in shape between simulated and measured reflectance. The morphological change in the spectrum can be caused when the distance between the probe and the tissue surface is not constant. A fixed distance is probably difficult to maintain in practice. However, a viable solution to this problem can be achieved through a proper mechanical design of the probe.

Despite this limitation, the proposed method provided a capability to evaluate tissue hypoxia and differentiate between intact and malignant tissues.

Additionally, the findings of this study are in good agreement with other works [24]. Bard et al. [25] found that endobroncho tumors were characterized by lower blood oxygenation. Also, Fawzy et al. [26] showed that malignant lesions had differences in blood volume fraction and oxygen saturation when compared to normal or benign lesions.

More importantly, our results confirm the association between tissue oxygen saturation and tissue transformation, in particular, tumor progression. Moreover, our findings, with regard to oxygen saturation levels resulted from the application of SD-DRS to oral tissue, are in accord with recent studies. For instance, a significant decrease in microvascular oxygenation in tumor tissue in comparison with healthy tissue was measured by Amelink et al. [27] as well as Stephen et al. [28]. As a result, SD-DRS offers high sensitivity to subtle changes in StO_2 making it a promising tool for accurate determination of tissue hypoxia in premalignant tissue, in particular, the contrast between tissue oxygenation in benign and malignant tissue. This may offer rapid noninvasive and biopsy-free diagnosis of suspicious lesions.

Accurate classification for the range of StO_2 values can be determined by investigating larger datasets of clinical measurement of diffuse reflectance spectroscopy from different stages of tissue transformation caused by malignancy or/and cancer. Although, in this study, acceptable differentiation between normal and benign tissue on the one hand ($p<0.0001$) and between normal and cancerous tissue on the other hand (($p<0.0001$)) have been attained. Differentiation between benign and cancer ($p=0.0272$) can be further improved using larger dataset for benign and malignant tumors. Another possible area of investigation is the application of the devised technique for retrieval of StO_2 from different types of cancer such as skin, breast, and cervical cancer to name but a few.

OSA CONTINUUM

As for scattering, the results of this study showed that scattering effect on the StO_2 estimated by SD-DRS is minimal and the variation of the StO_2 values can only account for up to a maximum of 4% as shown in Fig. 4(c). This is comparable to prior work of Hu et al. [13], they developed a simple radiometric analysis independent of scattering for quantification of tissue oxygenation using two wavelengths in the visible range.

Although our devised method is independent of scattering, it should be noted that the results presented in this work are subject to some uncertainties. That is, SD-DRS can be sensitive to the factors that may influence the measured spectra, for instance, alterations in probe pressure on the tissue surface affect absorption in tissue due to decreased hemoglobin as a result of increased pressure. Previous studies related to this issue have shown that the probe pressure significantly influences the reflectance and hence optical properties as well as physiological parameters extracted from diffuse reflectance spectra of biological tissues in vivo as reported by Popov et al. [29]. In vivo probe pressure effect on DRS was also investigated on different locations on human skin by Lim et al. [30]. They concluded that long-term probe pressure effects can have significant effects on physiological properties, even at the lowest pressure. while short-term (up to 2 s) light probe pressure effects are minimal. Their resulting clinical acquisition pressure is effectively less than the weight of the probe resting on the lesion. Thus, pressure effects on clinical measurements rest comfortably within the first two seconds of the pressure measurements as reported by them. For this paper, we assumed that the pressure effect on DRS is minimal and hence negligible. In addition, the problem of probe pressure should be mitigated by proper design of the DRS measuring probe in order to avoid errors in estimating parameters from DRS spectra and that is not only limited to BVF and StO_2 but also for all other optical properties and physiological parameters affected.

Another possible issue that may explain the variation in StO_2 extraction is that the second derivative is very sensitive to subtle changes in the diffuse reflectance. Thus preprocessing is essential for spectral analysis [31]. Savitzky-Golay (SG) filter was used in this paper as a preprocessing technique for smoothing the spectra. SG filter has more advantages over commonly used moving average filter. Also, SG filter can tract the spectrum more closely and account for transient effect in comparison with moving average filters. More importantly, it removes delays in the preprocessed spectrum at the beginning and end of the spectrum.

Since the proposed measuring method in this study relies heavily on second derivative, any noise in the spectra can be greatly amplified after taking derivatives and could lead to errors in area calculation and as a result inaccurate StO_2 level. Therefore, spectra should be smoothed before taking derivatives and applying this filter should be treated with caution to ensure adequate smoothing in the spectrum. In addition, SG filter is based on polynomial fitting while preserving the trends in the spectrum. SG filters performance can be controlled with two parameters: the window length of the filter (number of points to be considered) and the order of polynomial fitted to these points. In order to avoid any undesired attenuation in the spectrum after taking derivatives the window length can be adjusted. The larger the window length the greater the attenuation in the derivatives. This can be followed by adjusting the polynomial order as the maximum value for polynomial order must be one less than the window length. SG filter window length and polynomial order used in this study were 7 and 2 respectively. These values were found to be appropriate for the preprocessing of our simulated and measured diffuse reflectance spectra.

It is noteworthy to say that SD-DRS requires prior knowledge of total hemoglobin in order to reliably estimate StO_2 and possibly detect tissue hypoxia. Variation in the intensity of diffuse reflectance in the range from 500 to 600 nm can also be used as a spectral feature for determination of total hemoglobin concentration that can be used later for retrieval of StO_2 level from 2D matrix.

OSA CONTINUUM

All in all, the steps for implementing this method for StO_2 evaluation based on SD-DRS can be summarized by the flowchart given in Fig. 11. The developed approach only requires the investigation of diffuse reflectance over a relatively narrow spectral window of 100 nm. This is a major improvement over previous works such as Chen, P. et. al [12] where estimating of oxygen saturation required spectral information from different wavelengths or windows starting from 450 nm to 600 nm. This spectral region where Hb absorption is very strong and limits the volume of tissue investigated by DRS.

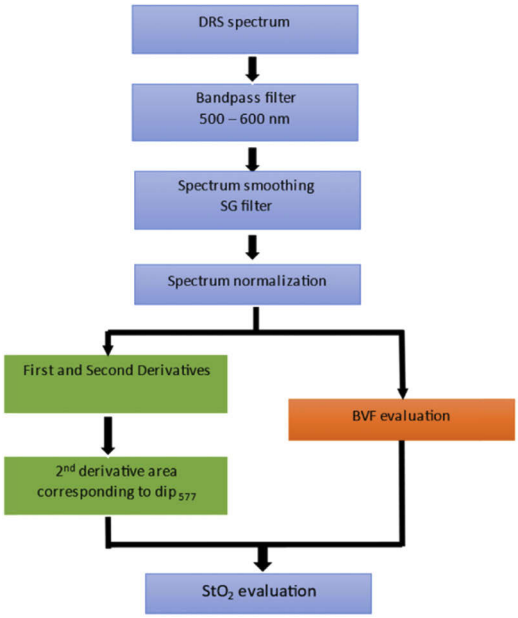

Fig. 11. Flowchart of the StO_2. evaluation scheme based on SD-DRS.

Although the findings presented in this study are of specific interest for tissue hypoxia in tumors, applying these outcomes to other disorders related to tissue oxygenation may result in better prognosis in other applications widely used in biomedical optics. That would open the way to further investigate other factors such as age, gender, etc. that may affect the tissue oxygenation in tissue and hence, offering important optical means for disease diagnosis, treatment and prognosis monitoring.

5. Conclusion

In summary, we have proposed a novel, independent of scattering, calibration-free and non-invasive spectroscopic method for evaluation of tissue hypoxia based on second derivative diffuse reflectance spectroscopy, the presented method was tested on simulated reflectance spectra and validated on clinical reflectance measurements. This opens the potential for low-cost, rapid and robust monitoring of tissue oxygenation non-invasively. Further research is needed to explore the potential applications of this method for differentiation and classification of different tissue pathologies other than oral malignancy. Clinical implementation of this approach for diagnostic and monitoring purposes where tissue oxygenation is required can also be pursuit as a next step forward.

Funding. Damascus University.

Disclosures. The authors declare no conflicts of interest.

OSA CONTINUUM

References

1. S. Bergstrand, M. A. Morales, G. Coppini, M. Larsson, and T. Strömberg, "The relationship between forearm skin speed-resolved perfusion and oxygen saturation, and finger arterial pulsation amplitudes, as indirect measures of endothelial function," Microcirculation **25**(2), e12422 (2018).
2. R. L. Siegel, K. D. Miller, and A. Jemal, "Cancer statistics, 2018," CA. Cancer J. Clin. **68**(1), 7–30 (2018).
3. P. Bickler, J. Feiner, M. Rollins, and L. Meng, "Tissue Oximetry and Clinical Outcomes," Anesth. Analg. **124**(1), 72–82 (2017).
4. G. Greisen, B. Andresen, A. M. Plomgaard, and S. Hyttel-Sørensen, "Cerebral oximetry in preterm infants: an agenda for research with a clear clinical goal," Neurophotonics **3**(3), 031407 (2016).
5. S. Kleiser, D. Ostojic, and N. Nasseri, "In vivo precision assessment of a near-infrared spectroscopy-based tissue oximeter (OxyPrem v1.3) in neonates considering systemic hemodynamic fluctuations," J. Biomed. Opt. **23**(06), 1–10 (2018).
6. A. I. Mundo, G. J. Greening, M. J. Fahr, L. N. Hale, E. A. Bullard, N. Rajaram, and T. J. Muldoon, "Diffuse reflectance spectroscopy to monitor murine colorectal tumor progression and therapeutic response," J. Biomed. Opt. **25**(03), 1–16 (2020).
7. L. Yu, Y. Wu, J. F. Dunn, and K. Murari, "In-vivo monitoring of tissue oxygen saturation in deep brain structures using a single fiber optical system," Biomed. Opt. Express **7**(11), 4685–4694 (2016).
8. P. Rejmstad, J. D. Johansson, N. Haj-Hosseini, and K. Wårdell, "A method for monitoring of oxygen saturation changes in brain tissue using diffuse reflectance spectroscopy," J. Biophotonics **10**(3), 446–455 (2017).
9. C. E. Cooper, C. E. Elwell, J. H. Meek, S. J. Matcher, J. S. Wyatt, M. Cope, and D. T. Delpy, "The noninvasive measurement of absolute cerebral deoxyhemoglobin concentration and mean optical path length in the neonatal brain by second derivative near infrared spectroscopy," Pediatr. Res. **39**(1), 32–38 (1996).
10. H. Z. Yeganeh, V. Toronov, J. T. Elliott, M. Diop, T.-Y. Lee, and K. St. Lawrence, "Broadband continuous-wave technique to measure baseline values and changes in the tissue chromophore concentrations," Biomed. Opt. Express **3**(11), 2761–2770 (2012).
11. S. G. B. de Koning, E. J. M. Baltussen, M. B. Karakullukcu, B. Dashtbozorg, L. A. Smit, R. Dirven, B. H. W. Hendriks, H. J. C. M. Sterenborg, and T. J. M. Ruers, "Toward complete oral cavity cancer resection using a handheld diffuse reflectance spectroscopy probe," J. Biomed. Opt. **23**(12), 1–8 (2018).
12. P.-C. Chen and W.-C. Lin, "Spectral-profile-based algorithm for hemoglobin oxygen saturation determination from diffuse reflectance spectra," Biomed. Opt. Express **2**(5), 1082–1096 (2011).
13. F. Hu, K. Vishwanath, J. Lo, A. Erkanli, C. Mulvey, W. T. Lee, and N. Ramanujam, "Rapid determination of oxygen saturation and vascularity for cancer detection," PLoS One **8**(12), e82977 (2013).
14. N. Nasseri, S. Kleiser, U. Wolf, and M. Wolf, "Tissue oximetry by diffusive reflective visible light spectroscopy: Comparison of algorithms and their robustness," J. Biophotonics **11**(9), e201700367 (2018).
15. N. Bosschaart, G. J. Edelman, M. C. G. Aalders, T. G. Van Leeuwen, and D. J. Faber, "A literature review and novel theoretical approach on the optical properties of whole blood," Lasers Med. Sci. **29**(2), 453–479 (2014).
16. R. Hennessy, S. L. Lim, M. K. Markey, and J. W. Tunnell, "Monte Carlo lookup table-based inverse model for extracting optical properties from tissue-simulating phantoms using diffuse reflectance spectroscopy," J. Biomed. Opt. **18**(3), 037003 (2013).
17. S. L. Jacques, "Optical properties of biological tissues: A review," Phys. Med. Biol. **58**(11), R37 (2013).
18. T. M. Bydlon, R. Nachabé, N. Ramanujam, H. J. C. M. Sterenborg, and B. H. W. Hendriks, "Chromophore based analyses of steady-state diffuse reflectance spectroscopy: Current status and perspectives for clinical adoption," J. Biophotonics **8**(1–2), 9–24 (2015).
19. K. W. Calabro and I. J. Bigio, "Influence of the phase function in generalized diffuse reflectance models: review of current formalisms and novel observations," J. Biomed. Opt. **19**(7), 075005 (2014).
20. R. Graaff, M. H. Koelink, F. F. M. de Mul, W. G. Zijlstra, A. C. M. Dassel, and J. G. Aarnoudse, "Condensed Monte Carlo simulations for the description of light transport," Appl. Opt. **32**(4), 426–434 (1993).
21. X. Zhong, X. Wen, and D. Zhu, "Lookup-table-based inverse model for human skin reflectance spectroscopy: two-layered Monte Carlo simulations and experiments," Opt. Express **22**(2), 1852–1864 (2014).
22. A. Amelink, H. J. C. M. Sterenborg, J. L. N. Roodenburg, and M. J. H. Witjes, "Non-invasive measurement of the microvascular properties of non-dysplastic and dysplastic oral leukoplakias by use of optical spectroscopy," Oral Oncol. **47**(12), 1165–1170 (2011).
23. J. A. Delgado, S. L. Jacques, and S. V. y Montiel, "Monte Carlo Modeling of Light Propagation in Neonatal Skin," in *Applications of Monte Carlo Methods in Biology, Medicine and Other Fields of Science* (IntechOpen, 2011) Chap. 17.
24. G. Einstein, K. Udayakumar, P. R. Aruna, D. Koteeswaran, and S. Ganesan, "Diffuse reflectance spectroscopy for monitoring physiological and morphological changes in oral cancer," Optik **127**(3), 1479–1485 (2016).
25. M. P. L. Bard, A. Amelink, M. Skurichina, M. Den Bakker, S. A. Burgers, J. P. Van Meerbeeck, R. P. W. Duin, J. G. J. V. Aerts, H. C. Hoogsteden, and H. J. C. M. Sterenborg, "Improving the specificity of fluorescence bronchoscopy for the analysis of neoplastic lesions of the bronchial tree by combination with optical spectroscopy: Preliminary communication," Lung Cancer **47**(1), 41–47 (2005).
26. Y. S. Fawzy, M. Petek, M. Tercelj, and H. Zeng, "In vivo assessment and evaluation of lung tissue morphologic and physiological changes from non-contact endoscopic reflectance spectroscopy for improving lung cancer detection," J. Biomed. Opt. **11**(4), 044003 (2006).

OSA CONTINUUM

27. A. Amelink, O. P. Kaspers, H. J. C. M. Sterenborg, J. E. van der Wal, J. L. N. Roodenburg, and M. J. H. Witjes, "Non-invasive measurement of the morphology and physiology of oral mucosa by use of optical spectroscopy," Oral Oncol. **44**(1), 65–71 (2008).
28. M. M. Stephen, J. L. Jayanthi, N. G. Unni, P. E. Kolady, V. T. Beena, P. Jeemon, and N. Subhash, "Diagnostic accuracy of diffuse reflectance imaging for early detection of pre-malignant and malignant changes in the oral cavity: A feasibility study," BMC Cancer **13**(1), 278 (2013).
29. A. P. Popov, A. V. Bykov, and I. V. Meglinski, "Influence of probe pressure on diffuse reflectance spectra of human skin measured in vivo," J. Biomed. Opt. **22**(11), 1–4 (2017).
30. L. Lim, B. Nichols, N. Rajaram, and J. W. Tunnell, "Probe pressure effects on human skin diffuse reflectance and fluorescence spectroscopy measurements," J. Biomed. Opt. **16**(1), 011012 (2011).
31. Å. Rinnan, F. van den Berg, and S. B. Engelsen, "Review of the most common pre-processing techniques for near-infrared spectra," TrAC, Trends Anal. Chem. **28**(10), 1201–1222 (2009).